Journal Pre-proof

Optical properties from extinction cross-section of single pollen particles under laboratory-controlled relative humidity

A. Valenzuela, F.J. García-Izquierdo, G. Sánchez-Jiménez, E. Bazo, J.L. Guerrero-Rascado, P. Cariñanos, L. Alados-Arboledas, F.J. Olmo-Reyes

PII: S0021-8502(23)00176-3

DOI: https://doi.org/10.1016/j.jaerosci.2023.106311

Reference: AS 106311

To appear in: *Journal of Aerosol Science*

Received Date: 16 August 2023

Revised Date: 20 November 2023

Accepted Date: 28 November 2023

Please cite this article as: Valenzuela A, García-Izquierdo FJ, Sánchez-Jiménez G, Bazo E, Guerrero-Rascado JL, Cariñanos P, Alados-Arboledas L, Olmo-Reyes FJ, Optical properties from extinction cross-section of single pollen particles under laboratory-controlled relative humidity, *Journal of Aerosol Science* (2024), doi: https://doi.org/10.1016/j.jaerosci.2023.106311.

Optical properties from extinction cross-section of single pollen particles under laboratory-controlled relative humidity

A. Valenzuela[+,‡,*], F.J. García-Izquierdo[+,‡], G. Sánchez-Jiménez[+], E. Bazo[+,‡], J.L. Guerrero-Rascado[+,‡], P. Cariñanos[+,ℵ], L. Alados-Arboledas[+,‡] and F.J. Olmo-Reyes[+,‡]

[+]Andalusian Institute for Earth System Research (IISTA-CEAMA), Granada 18006, Spain
[‡]Department of Applied Physics, University of Granada, Granada 18071, Spain
[ℵ]Department of Botany, University of Granada, Granada 18071, Spain

ABSTRACT: A growing body of research suggests that pollen suspended in the atmosphere have a major environmental and climatic impact. However, our current knowledge of pollen is rather limited with respect to its extinction capacity, its optical properties and how these vary with atmospheric water content. Understanding their water absorption capacity can improve our understanding of their radiative effects and, thus, improve climate models. In this work, an electrodynamic Paul trap was coupled to a cavity ring down spectroscopy (CRDS) to directly measure the ring down time (τ) of four individual types of pollen particles: *Olea*, *Fraxinus*, *Populus* and *Salix* exposed to changing relative humidity (RH). Resonant structures in τ values between ~ 90-45 % RH indicated that pollen was wettable at high RHs. τ was used to calculate light extinction cross-section (σ_{ext}) at 532 nm as a function of RH. Optical growth factor (f_{RH}) was evaluated as the ratio between $\sigma_{ext}(\sim 80\%\, RH)$ and $\sigma_{ext}(dry)$. From f_{RH}, the semi-empirical single hygroscopicity parameter (κ_{emp}) was found to be 0.038-0.058 for the four pollen types. Under controllable treatment of the water content and an adequate selection of complex refractive index (m), CRDS-σ_{ext} data was fitted to theoretical σ_{ext} from Mie theory. The reasonable agreement achieved allowed for gaining knowledge about the m and how particle size shrugged during dehydration. As a result, a climate-lowering effect of *Olea* pollen particles, which contain a fraction of scattered aerosol, should be considered in the models.

KEYWORDS: pollen, single aerosol particle, optical properties, hygroscopicity, radiative effects.

SYNOPSIS: This study provides optical properties of pollen (complex refractive index) and their dependence on water content, which has environmental relevance from the point of view of radiative effects.

1. INTRODUCTION

Although primary biological aerosol particles (PBAPs) represent a small fraction of the total aerosol burden in the atmosphere, their annual emission fluxes are estimated to be up to 1000 Tg yr^{-1} and they are thought to have a significant impact on human health and climate (Stocker et al., 2013; Zhang et al., 2021). PBAPs could modify the atmospheric-surface radiative forcing by interacting with light through scattering and absorption processes and by acting as cloud condensation nuclei (Pope, 2010; Zhang et al., 2021). However, their physicochemical properties are among one of the most uncertain quantities for the aerosol scientific community, which limits our ability to evaluate their radiative effects (Després et al., 2012; Martin et al., 2010). PBAPs that can be found in the atmosphere include pollen, bacteria, fungal spores, algae, mosses and ferns, viruses, and fragments of animals and plants (Deguillaume et al., 2008; Després et al., 2012; Möhler et al., 2007; Moller et al., 2008).

Pollen is one of the most abundant and the largest PBAPs and its emission flux and atmospheric concentrations are around 47-84 Tg $year^{-1}$ (Després et al., 2012; Fröhlich-Nowoisky et al., 2016; Matthias-Maser et al., 2000). A great number of pollen or sub-pollen particles are present in urban environments mainly in warmer seasons. Because of climate change, the period of the pollen season should be extended, affecting wider extended geographical areas (Bielory et al., 2012; Ziska et al., 2011). Much of the work on pollen has focused on the determination of the hygroscopic kappa parameter (κ). At undersaturated relative humidity (RH) conditions, κ determines the ability of particles to absorb water (Petters and Kreidenweis, 2007). Using an electrodynamic balance, Pope (2010) calculated the mass growth factor (M/M_0), where M and M_0 are the masses of pollen in a specific RH and in dry conditions, respectively. On this analysis the hygroscopic response was parameterized using $\kappa-$Köhler theory providing values of κ between 0.05 and 0.1 for four different types of pollen (*Narcissus*, *Betula*, *Salix*, *Juglans*). Following the same procedure, Griffiths et al. (2012) found that the pollen was moderately hygroscopic and its surface wettable at high humidities. In addition, there was no hysteresis observed within the humidograms and due to their large grain size, they concluded that pollen grains are efficient cloud condensation nuclei (Diehl et al., 2001; Pope, 2010). The temperature effect (5-37 °C) on pollen hygroscopicity was estimated to be small for six pollen species with κ values ranging from 0.034-0.061 at 25°C by Tang et al. (2019). Therefore, the no significant differences found on κ makes it very challenging to use as a pollen identifier and hence, highly sensitive techniques are demanded for this aim.

From how light interacts through scattering and absorbing processes with matter we can extract previously unseen information about the particle microphysical state and chemical composition during changing environmental conditions and how this translates into aerosol properties. These effects on light are quantified by the scattering cross section (σ_{scat}) and the absorbing cross section (σ_{abs}) parameters. The real part (n) of the complex refractive index (m) impacts on scattering radiative processes and the imaginary part (k) of m is involved in how the light absorbing processes occur being the following equation:

$$m = n + ik \quad (1)$$

Experimental light elastic scattering (phase function) is a consolidated approach very widely used as a product to gain information about size distributions, morphologies and n (David et al., 2016; L. Price et al., 2020). To our knowledge, only a few studies provided values of n and k for pollen in real atmospheres. For instance, in the literature we found that n for *Cupressus* pollen was estimated to be in the range 1.3-1.54, while k was close to zero (Ebert et al., 2002; Gómez Martín et al., 2021; Kim et al., 2018). Nevertheless, non-zero values for k, ranging between 0.01-0.2, was found by Hu et al. (2019) using experimental reflectance measurements for twelve biomaterials in the spectral range from 0.24 to 14 μm. Methodologies based on interferometry, light scattering or laser-induced fluorescence were developed for pollen classification (Kiselev et al., 2013; Pan et al., 2011). Light scattering techniques provide rapid, non-invasive, and extremely sensitive sampling of small but significant biological changes that cannot be differentiated by any other optical technique (Bickel and Stafford, 1980; Cholleton et al., 2022a; Gómez Martín et al., 2021). Cholleton et al. (2022) established a technique to detect and differentiate among the existing four pollen taxa (*Fraxinus*, *Betula*, *Ambrosia*, *Pinus*) using 10 scattering matrix elements. They exhibited clearly different light-scattering characteristics, which allowed differentiation between each pollen type. Nevertheless, these experiments were carried out under dry pollen conditions (< 10% RH). It would be crucial to extend the analysis to changing environmental conditions.

There is much controversy about the geometry of the shape of pollen grains and its effect on light scattering properties. In this sense, remote sensing platforms such as the lidar were used to identify pollen types based mainly on their non-spherical geometry through the particle linear depolarization ratio (δ_L) (Córdoba-Jabonero et al., 2018; Noh et al., 2013a, 2013b; Sassen, 2008; Shang et al., 2020; Sicard et al., 2016). Nevertheless, other studies stated that δ_L calculated from lidar measurements cannot be used to differentiate between particle types, not even regarding size because different aerosol types in the visible spectral range show similar average value of δ_L (180°) (Gómez Martín et al., 2021). These same authors suggested that the light scattering of *Cupressus* pollen can be modelled as if it were near spheroid with a very low aspect ratio.

An added difficulty to the above issues is that observations in the environment are complicated by the uncontrollable nature of the atmosphere (Huffman and Santarpia, 2017; Santarpia, 2016). The study of aerosols often involves the study of the average behaviour of samples, which makes it difficult to accurately quantify stimulus-response relationships to the extent necessary for rigorous predictive modelling. In this regard, laboratory studies are necessary to understand how microphysical state, chemical composition and transformation timescales are quantified in controlled laboratory measurements (Krieger et al., 2012). Hence, along with the challenge of analysing aerosol samples, there is a strong motivation to develop single-particle monitoring techniques (Fernandez et al., 2019; Hopkins et al., 2004; Pope, 2010; Redding and Pan, 2015a, 2015b). One of the main advantages of single-particle analysis is that an individual particle can be confined to a fixed position in space; consequently, it can be indefinitely interrogated by various optical detection techniques, such as light scattering, Raman spectroscopy or fluorescence (O'Connor et al., 2011; Swanson et al., 2023; Walker et al., 2013; Wang et al., 2015, 2019). Working with single particles light elastic scattering builds an interference structure in the far-field between light passing through a particle and that passing close to the edge that can be collected and fitted to Lorenz-Mie theory to estimate its size (Cotterell et al., 2017, 2015; Mason et al., 2015; Valenzuela et al., 2020). A limitation arises with this approach when particle absorbs light, or it is not a perfect sphere because the phase function loses contrast. To overcome this drawback, a window of opportunity opens in the bioaerosol field if extinction cross section (σ_{ext}) data become available, which will contain invaluable information on physicochemical properties, particle geometries and light absorption. Recent advances in the aerosol spectroscopy field allowed for evaluating continuous σ_{ext} measurements after a single inorganic salt experimented efflorescence, coupling a Cavity Ring Down Spectrometer (CRDS) to a linear electrodynamic quadrupole (Valenzuela et al., 2021). By fitting CRDS-σ_{ext} values to theoretical σ_{ext} modelled by spheroid code, an aspect ratio mean value of the irregular crystallised particle was estimated. Based on the latter configuration, Knight et al. (2022) successfully obtained the evolution of k for two-component droplet composed of nigrosine and 1,2,6-hexanetriol. Of significant importance is to find out how n is modified with water content in the particle which will help to one more precise quantification of its radiative effects. Valenzuela et al. (2018) established that for standard uncertainty in n of ± 0.02 the uncertainty in estimating the radiative forcing efficiency (RFE) was ± 25% at 90% RH for ammonium sulphate (AS) aerosol. Further, focusing on single particles, the accuracy in estimating of n at 532 nm was raised to ± 0.003 which translated to a more precise estimation of the RFE ± 5% for the above compound. In short, the electrodynamic trap coupled to CRDS can provide extraordinary details, so far unrevealed, about the properties of pollen that would complement the analysis already performed.

In this work we advance a new configuration, coupling a Paul Electrodynamic Trap (PET) with a Cavity Ring Down Spectroscopy CRDS. The novel setup is a versatile working platform, adding enormous flexibility by optically interrogating the same trapped particle over time with excellent stability and reproducibility. This advantage was exploited to direct calculation of σ_{ext} and then optical properties of single pollen particles as well as their radiative effects. The n and k were calculated and their dependence on RH was evaluated. We focus on *Olea*, *Fraxinus*, *Populus* and *Salix* pollen types, all of them from plant species representative of the Mediterranean bioclimatic region.

2. EXPERIMENTAL SETUP

2.1 Paul Electrodynamic Trap

A Paul Electrodynamic Trap (PET) is located inside a custom-made chamber under atmospheric pressure and room temperature, with all measurements performed around 295 K (Figure 1). This platform is formed by two conical electrodes separated by 1.5 mm that are enclosed by grounded cylindrical shields, which have a diameter of 2 and 3 cm of length. An AC voltage signal is applied to the cones; the typical operation amplitude range of the AC field is between 1 kVpp and 2 kVpp at a frequency ranging from 1 to 2 kHz. Establishing the above values, the PET is capable of trapping particles ranging between 700 nm up to a few micrometres in radius. A CMOS camera (Thorlabs, DCC1546M) coupled to a 20× long working distance lens (Mitutoyo) with a numerical aperture (NA) of 0.42, oriented at 90° to the optical cavity, is used to control the particle position from a phase function image at 473 nm wavelength. The principle of operation of the Paul electrodynamic trap is explained in detail by Valenzuela et al. (2020).

2.2 Relative humidity control

RH is one the most important atmospheric parameters, which plays a key role in aerosol physical conditions. A RH is achieved in a nitrogen flow by mixing wet and dry gas in controlled ratios. A nitrogen cylinder is regulated to a pressure of 3 bar and used at this inlet pressure to supply two mass flow controllers (MFC) in parallel (MKS GE50A, rated for 500 sccm N_2) both powered by a MKS power supply (MKS-946-EU-FCFCNA-NA). The RH inside the trapping cell is monitored using a capacitance probe (Honeywell).

2.3 Cavity ring down spectroscopy: ring down time and optical properties

Here, a Cavity Ring Down Spectrometer (CRDS) is employed to calculate σ_{ext} of single particles by mean of careful manipulation of the PET with a continuous single-mode laser (Laser Quantum Torus) at 532 nm wavelength (Figure 1). σ_{ext} is calculated from equation:

$$\sigma_{ext} = \frac{\pi w_0^2 L}{2c}\left(\frac{1}{\tau} - \frac{1}{\tau_0}\right) \quad (2)$$

where τ_0 and τ are the ring-down times with empty cavity and when it contains particle, respectively, w_0 is the estimated beam waist, L is the length of the cavity and c is the speed of light. More details about cavity ring down time methodology can be found in Supporting Information.

The variation in r and n was determined by fitting the complete measured $\sigma_{ext,1Hz}$ data set to theoretical σ_{ext} calculated using the Mie theory in a self-consistent step. For all hygroscopic response measurements reported in this study, the n varied with the particle size. Therefore, we parameterised n in terms of particle radius using the expression:

$$n = n_0 + \frac{n_1}{r^3} + \frac{n_2}{r^6} \quad (3)$$

in which r was the particle radius, n_1 and n_2 were fitting parameters, and n_0 (1.335) was the real refractive index of pure water at 532 nm wavelength. This procedure was previously tested to obtain the n of NaCl as a function of RH (Figure S1, Supporting Information).

The best fit was calculated using the reduced cumulative fractional difference (CFD_R)(Zarzana et al., 2012):

$$CFD_R = \frac{1}{N}\sum_{i=1}^{N} \frac{|\sigma_{ext,Mie} - \sigma_{ext,1Hz}|}{\sigma_{ext,1Hz}} \quad (4)$$

where $\sigma_{ext,Mie}$ was the theoretical extinction cross section and N was the number of different particle radius used. The CFD_R was calculated for a wide range of n and r values, and the value of n and r that gave the lowest CFD_R were taken to be these for the pollen as function of RH. A fixed non-zero value for k provided a lowest CFD_R for each pollen type.

To determine the hygroscopic behaviour of pollen a semi-empirical relationship for κ was proposed by Dawson et al. for evaluating different water-soluble sugars from cavity ring down data (Dawson et al., 2020):

$$\kappa_{empirical} = \left(f_{RH}(\sim 80\%RH, dry)^{\frac{3x0.28}{0.86}} - 1\right)\left(\frac{1-RH/100}{RH/100}\right) \quad (5)$$

where the optical growth factor (fRH) was calculated in this study by dividing the $\sigma_{ext,w}$ of the humidified particle by the $\sigma_{ext,d}$ of the dry particle:

$$f_{RH}(w,d) = \frac{\sigma_{ext,w}}{\sigma_{ext,d}} \quad (6)$$

where w was the RH of the humidified particle and d was the RH of the dry particle. We assumed that semi-empirical relationship was applicable to our study. We considered the value of the humidified $\sigma_{ext,w}$ at around 80% RH and the value of $\sigma_{ext,d}$ as dry RH % when the pollen particle no longer loses water according to our analysis.

Detailed explanations of the operation of the Paul electrodynamic trap coupled to the cavity ring down spectroscopy setup are given by Valenzuela et al. (2024).

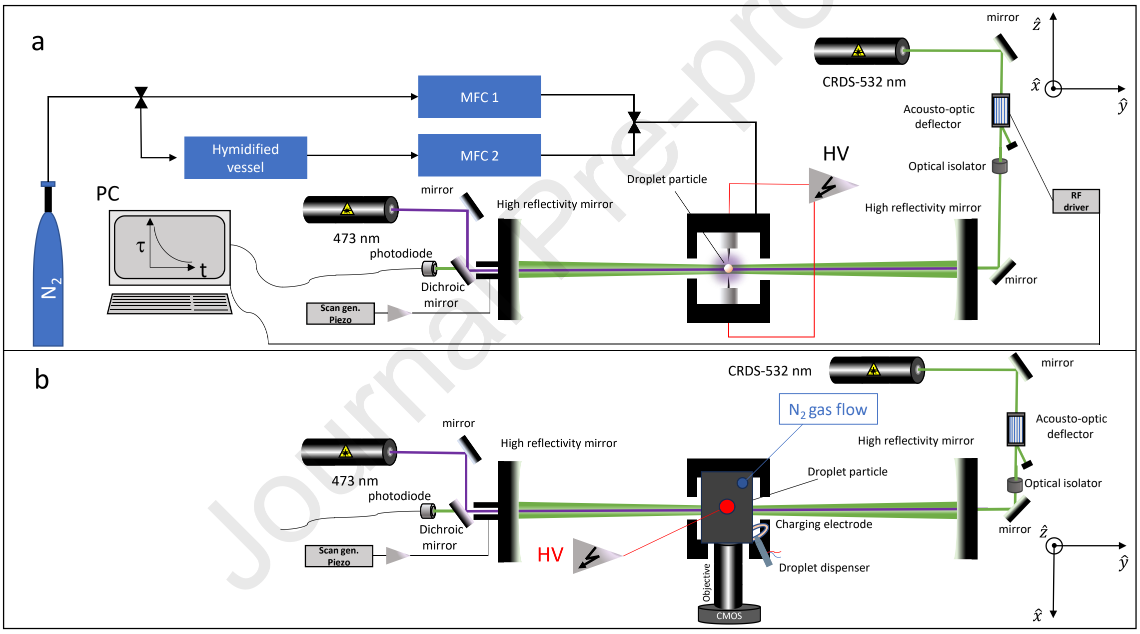

Figure 1. a) Scheme of cavity ring down spectroscopy setup, relativity humidity system and the Paul Electrodynamic Trap (PET) seen from front and b) seen from top.

2.4 Harvesting and laboratory preparation of pollen samples

For the measurements we used four different pollen samples: *Olea*, *Fraxinus*, *Populus*, and *Salix*. Optical microscope images about four single pollen particle types are showed in Figure 2. Then, flowers of *Olea* and *Fraxinus* and catkins from *Salix* and *Populus* were collected in the period immediately to anthesis, that is, prior to the opening of the anthers. Afterwards, the flowers were dried at room temperature (approximately 20ºC) for 48 hours and sieved to facilitate the extraction of pollen and eliminate possible plant remains. The amount of pollen obtained was approximately 2 g per species, that was stored in microtubes in a refrigerator at 4ºC to avoid the oxidation and degradation process (Ramírez-Aliaga et al., 2022). The preparation of the pollen washing water was performed as follow: first, we suspended 1 g of pollen in 20 ml of deionized water. After shaking the suspension, it was placed in a glass bottle in the refrigerator overnight. The next day, the suspension was shaken again before being delivery in the PET chamber.

The experimental process was composed of following steps: (1) desired RH conditions were established inside the PET chamber, (2) a droplet dispenser (Microfab, 20(MJ-ABP-01)) was used to delivery droplets inside the PET chamber and (3) RH was steady gone down with a controlled gas flow ratio between two mass flow controllers. We routinely measured deliquescence relative humidities (DRHs) of NaCl and $(NH_4)_2SO_4$ to inspect the RH accuracy of the humidity sensor, and the difference between measured and theoretical DRHs did not exceed 1%.

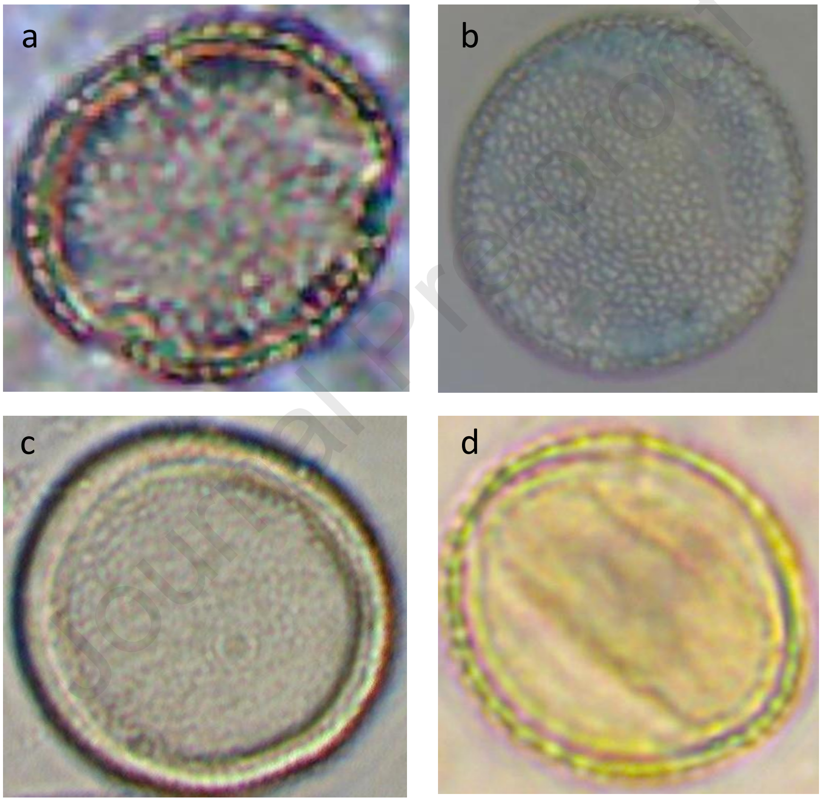

Figure 2. Optical microscope images of a) *Olea*, b) *Fraxinus*, c) *Populus* and d) *Salix* (Images from P. Cariñanos).

3. Results and discussion

3.1 Cavity ring down time data and hygroscopic behaviour

Single aqueous aerosol containing one of the pollen particles were trapped at high RH (~80-90%). A droplet dispenser was used to deliver particle causing that RH is unsteady. It was necessary to wait about five minutes before proceeding with data collection where, once the RH was stabilized, it was progressively reduced at a rate of 1% per minute until the measured τ showed constant values even though the RH continued to decrease. Repeat measurements were performed for each pollen type: *Olea* (4), *Fraximus* (2), *Populus* (2) and *Salix* (2).

The procedure followed to collect data under RH changes for the four types of pollen was equivalent. We focus in τ measurements and hygroscopic response for one single *Olea* pollen particle to explain the process. The *Olea* pollen was initially captured at an RH of around 90% (Figure 3a) and the change in τ was monitored over a time scale of ∼6300 s as the RH is allowed to reduce (Figure 3b).

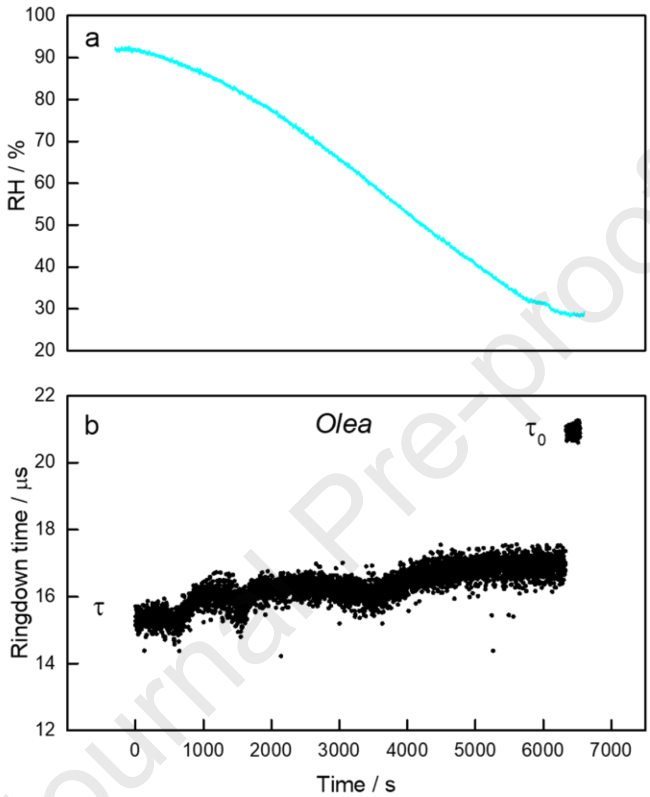

Figure 3. a) Decrease of RH and b) evolution of τ during the evaporation of an *Olea* pollen particle.

The first change we observed was a moderate increase in τ, which can only be explained by the fact that during the dehydration process, the particle lost water and reduced its size. In addition, this increase in τ was accompanied by fluctuations with different resonance peaks related to the fact that during the evaporation process the particle reached specific sizes for which it behaves as an optical cavity resonant with the laser wavelength. This trend in τ occurred until the RH was reduced to ~ 45%. From this point on, τ remains constant, indicating that the particle no longer lost water and is assumed to be dry. An envelope of measured τ values resulting from the Brownian motion of the particle passing through different phases of the standing wave, corresponding to the boundaries of the envelope to the particle centred at a node or at an antinode. Furthermore, since there was no loss of contrast in the experimental phase function image (Figure 4) at 473 nm wavelength after RH~ 45%, this can be interpreted to mean that the particle continued to show a spherical shape. This hypothesis is also supported by the behaviour of τ, since it did not show an abrupt change that would lead one to suspect an irregular shape of the particle. Therefore, we can hypothesize that Mie theory is a good approximation to fit our experimental data contrary to the results reported in previous studies where a non-spherical assumption is considered.

Figure 4. Phase function image of a single *Olea* particle at 473 nm wavelength and 40% RH (Image from A. Valenzuela).

3.2 Light extinction cross sections and optical properties of pollen particles

The measured σ_{ext} were compared to Mie σ_{ext} theoretical calculations using the procedure described in Sect. 2.3. Figures 5a, b, c, and d show example σ_{ext} data sets measured and the best-fit $\sigma_{ext,Mie}$ envelopes for four single pollen particle types. The σ_{ext} data sets have between 1-3 resonance features depending on the pollen type even though the particles evaporated over very similar radius and RH ranges, likely owing to different hygroscopic behaviour. Overall, the trend of σ_{ext} is explained, in addition to the shrinking in size, also by the change on refractive index of the particles. As RH is decreased, σ_{ext} is expected to decrease because the geometric cross section of particle becomes smaller. The extinction capacity decreased between ~20 and 28 % for *Olea* and *Salix* pollens, respectively, when RH decreased from 80% to 45% (Figures 5a and d). The hygroscopic behaviour could play a significant role from point of view of radiative effects. In the case of *Fraxinus* and *Populus* pollens, the extinction capacities decreased between 14 and 8 %, respectively (Figures 5b and c). We take advantage of the occurrence of resonant peaks for comparing with Mie theory and gain knowledge in optical properties.

Figures 5 e-h show n and r values as a function of the RH for individual pollen particles. As the RH was reduced, r decreased due to water loss and n increased because the solute became more concentrated within the aqueous droplets. The n for *Olea* and *Salix* pollens showed similar values in each RH interval, with the difference between the values for each pollen being less than the standard deviation within each pollen type. In the case of *Olea* pollen, the r is reduced ~ 120 nm and n ranges from 1.54 to 1.65 (Figure 5e). Since we assumed that the k of water was zero, we fixed a k value during the fitting process of

n and r for the whole range of RH. We tested for a set of different k values finding the lowest CFD for a k value of 0.00109 for *Olea* pollen. We conclude that *Olea* pollen was not very absorbing of light at 532 nm wavelength. The n for *Populus* pollen showed less variability with RH with values ranging from 1.53 to 1.56, which is indicative of its low hygroscopicity (Figure 5 g). *Fraxinus* pollen showed the lowest k value among the four pollen types with a value of 0.0007. Given the complexity of working with pollen grains no information about n and k values and their dependence with RH are reported in the literature. In general, the m values we have reported have lighter absorption and moderate scattering components than other aerosol types, e.g., mineral dust.

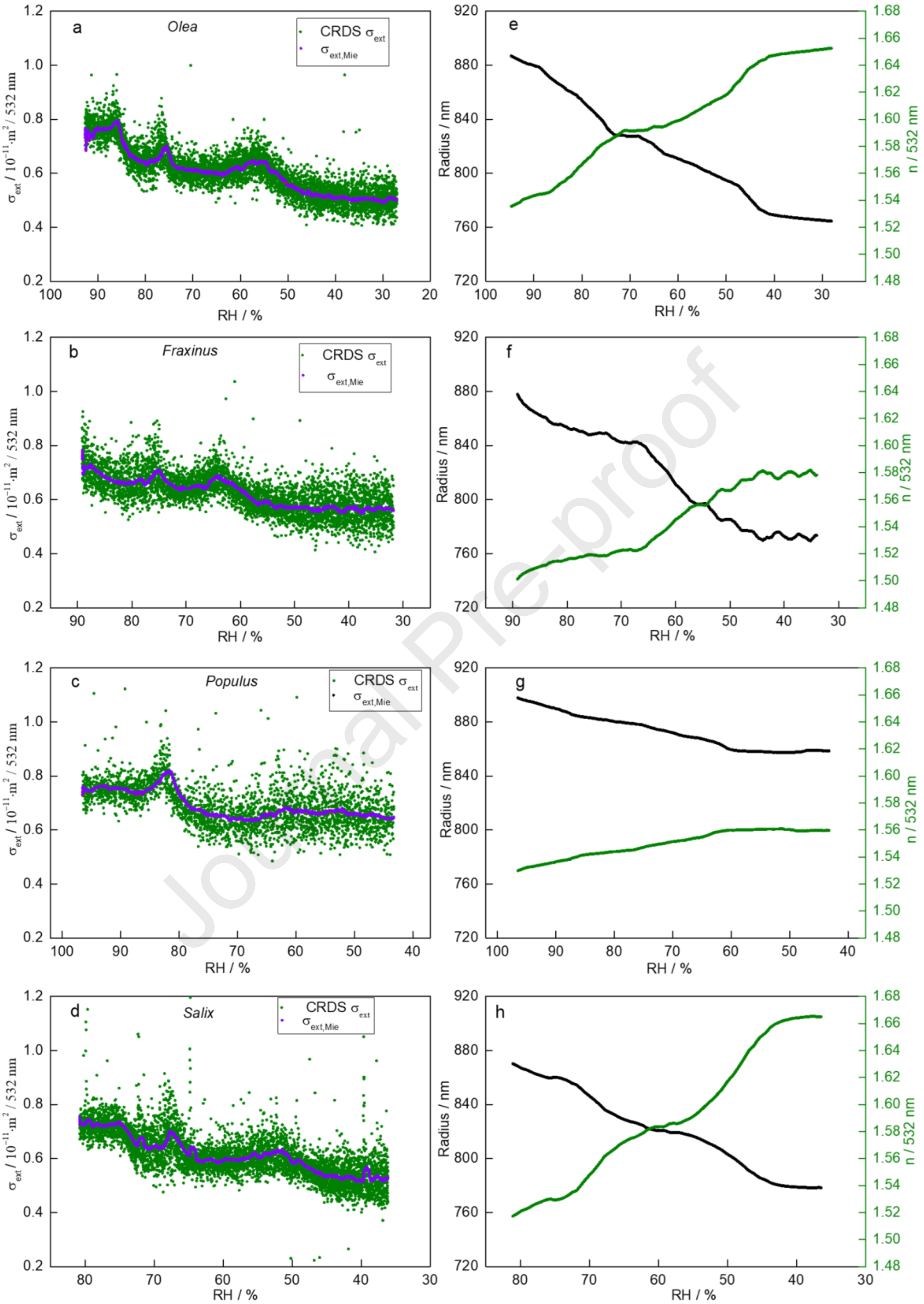

344 **Figure 5**. a, b, c, and d) Measured σ_{ext} (green dots) and fitted σ_{ext} (purple dots) as function of RH and e,
345 f, g, and h) calculated n and r values as function of RH for *Olea*, *Fraxinus*, *Populus* and *Salix* pollen
346 respectively.

347

Table 1 reports the calculated n values as function of the RH for each pollen species. For each type, we performed between 2 and 4 individual experiments and the n was fit separately for each experiment. The number of individual particles to average n are included. The reported values and errors are the averages and standard deviations from the individual fits for each pollen types. All CFD values were less than 0.003, which indicates that the fitted n and r values agree with measured data to within 0.3%.

RH%	*Olea* (4) [+]	*Fraxinus* (2) [+]	*Populus* (2) [+]	*Salix* (2) [+]
	$k \pm \Delta k$			
	0.0012± 0.0001	0.0007± 0.0001	0.0009± 0.0001	0.0010± 0.0001
	$n \pm \Delta n$			
90	1.545 ± 0.010	1.503 ± 0.012	1.537 ± 0.011	--
80	1.570 ± 0.013	1.516 ± 0.013	1.549 ± 0.032	1.520 ± 0.011
70	1.581 ± 0.017	1.522 ± 0.011	1.552 ± 0.012	1.547 ± 0.022
60	1.589 ± 0.021	1.545 ± 0.023	1.559 ± 0.021	1.584 ± 0.014
50	1.602 ± 0.018	1.567 ± 0.021	1.561 ± 0.015	1.616 ± 0.019
40	1.621 ± 0.021	1.578 ± 0.018	1.563 ± 0.014	1.664 ± 0.024

[+]Note: In parenthesis the number of particles used for averaging.

Table 1. n and k values as function of RH retrieved in this study. The reported values and errors are the averages and standard deviations from the individual fits for each pollen types. All values are for λ = 532 nm.

To verify the goodness of our system to determine the hygroscopic behaviour of pollen, we evaluated $f_{RH}(\sim 80\%RH, dry)$ of ammonium sulphate at 80% RH from CRDS data at 532 nm wavelength for dry particle of ~ 0.9 μm in radius. The result provided a value for $f_{RH}(\sim 80\%RH, dry)$ and κ_{emp} of 1.83 ± 0.21 and 0.34 ± 0.06, respectively, that shows good agreement when compared to Mie theory and besides these are consistent with data provided in the literature (Garland et al., 2007).

Mean f_{RH} value was determined for each of the pollen types from measured σ_{ext} values. Our study found that maximum $f_{RH}(\sim 80\%RH, dry)$ mean value was for *Salix* with 1.39 ± 0.11 for dry radius particle of ~ 0.77 μm being the minimum for *Fraxinus* with a mean value of 1.15 ± 0.03 for dry radius particle of ~ 0.81 μm. The f_{RH} decreased with increasing dry particle size. It is because extinction cross sections increase nonlinearly with particle radius, with a more pronounced increase at the smaller sizes. The conversion of f_{RH} to κ_{emp} allows a direct comparison between different pollen species. For CRDS derived κ_{emp} values, the error in individual experiment comes from uncertainties in RH measurements and in the fact that we work with σ_{ext} measurements of a standing wave which has a width in its values due to the interaction of the particle with the extremes of the wave, node, and antinode and with intermediate values. The mean values of κ_{emp} ranged between maximum values of 0.058 ± 0.012 and 0.057 ± 0.007 for *Salix* and

Olea, respectively, and minimum values of 0.038 ± 0.005 and 0.039 ± 0.006 for *Fraxinus* and *Populus*, respectively. The range of values found for κ_{emp} lie within the range of values provided by other authors for pollen species (Pope, 2010; Tang et al., 2019).

4. Atmospheric Implications

Radiative forcing efficiency. The imaginary refractive index (k) is a unitless value related to the light absorption capacity of the particle. In our analysis this quantity is not very large for all pollen species, but it is non-zero; therefore, pollen particles scatter and absorb light. We evaluated how this affects the radiative forcing with respect to a pure scattering particle such as ammonium sulphate (AS). Noll&Khalili (1988) have shown that sulphates and nitrates, among other elements, adhere to the surface of some pollen. A refined treatment for n as a function of RH was given by Valenzuela et al. (2018). To our knowledge, scarce studies have evaluated the radiative effects of pollen and even less considering its dependence on RH. Since the range of *n* for each pollen type is from 1.505 for *Fraxinus* at 40%RH to 1.66 for S*alix* at 90%RH, we have chosen *Olea* pollen as representative of the other pollen types because we do not expect the radiation effects to vary too much since *n* does not vary too much between the different pollen types.

For aerosol consisting of an internal mixture of 20% AS and 80% pollen by volume (like that used in Prisle et al. (2019)), the complex refractive index (m) was calculated following the procedure given by Robinson et al. (2013):

$$m_{Olea,AS,w} = \frac{V_{AS}m_{AS}+V_{Olea}m_{Olea}}{V_{AS}+V_{Olea}} \quad (7)$$

where w refers to water, $m_{Olea,AS,w}$ was the complex refractive index of the internal mixture with *Olea*, AS and water, $m_{Olea,w}$ was the complex refractive index of *Olea* and water and $m_{AS,w}$ was the complex refractive index of AS and water. These values are listed in Table 2. The procedure for calculating m and parameterizing the radius is explained in Supplementary Material. We considered in our study that *Olea* pollen grains were spherical applying Mie theory. All calculations were performed at 532 nm because optical properties were retrieved on this wavelength and besides it is representative of the solar visible spectrum. From our analysis we assumed an effective dry radius for *Olea* of 0.77 µm. The input parameters used to supply the Mie code were m, k and the size parameter (x) calculated for spherical particles as:

$$\mathrm{x} = \frac{2 \cdot \pi \cdot \mathrm{r}}{\lambda} \quad (8)$$

where r is the particle radius at the specific RH and λ is 532 nm wavelength.

In our study, the following aerosol radiative properties were calculated: the extinction efficiency (Q_{ext}), single scattering albedo (ϖ), asymmetry parameter (g) and backscattering fraction (β) including dependence on particle size, composition, RH and wavelength. These optical parameters were necessary to estimate the RFE at the top of the atmosphere caused by a thin aerosol layer in the lower troposphere from the equation proposed by Haywood and Shine (1995). Some previous publications have reported the use of this treatment to study the RFE (Dinar et al., 2008; Erlick et al., 2011; Haywood and Boucher, 2000; Randles et al., 2004; Valenzuela et al., 2018; Zarzana et al., 2014).

Our calculations of RFE are derived using the same equations and base-level assumptions as those by Erlick et al. (2011).

$$\mathrm{RFE} = \frac{\Delta \mathrm{F}}{\mathrm{AOD}} = \mathrm{SD}(1\text{-}\mathrm{A_{cld}})\mathrm{T_{atm}^2}(1\text{-}\mathrm{R_{sfc}})^2 \left[2\mathrm{R_{sfc}} \frac{1\text{-}\overline{\omega}}{(1\text{-}\mathrm{R_{sfc}})^2} \text{-} \beta\overline{\omega}\right] \quad (9)$$

where ΔF is the radiative forcing, AOD is the aerosol optical depth, S is the solar constant (set to 1370 W m^{-2}). For the rest of the parameters, we assumed the standard condition of a continental area. D is the fractional day length (set to 0.5), A_{cld} is the fractional cloud cover (set to 0.61), T_{atm} is the solar atmospheric transmittance (set to 0.76), and R_{sfc} is the surface albedo (set to 0.15). β is a function of hemispheric backscatter fraction b, defined as the ratio of backscattering efficiency to total scattering efficiency and $\overline{\omega}$ is the single scattering albedo caused by a uniform and optically thin aerosol layer. The parameter β was calculated from the Henyey–Greenstein phase function:

$$\beta = 0.082 + 1.85 \cdot \mathrm{b} \text{-} 2.97 \cdot \mathrm{b}^2 \quad (10)$$

whereas b was derived from g through the equation (Wiscombe and Grams, 1976):

$$\mathrm{b} = \frac{1\text{-}\mathrm{g}^2}{2\mathrm{g}}\left(\frac{1}{\sqrt{1+\mathrm{g}^2}} \text{-} \frac{1}{\sqrt{1+\mathrm{g}}}\right) \quad (11)$$

The results of the RFE calculations are shown in Table 2.

$RH\%$	$m_{AS,w}$ [a]	$m_{Olea,w}$ [b]	$m_{Olea,AS,w}$ [b]	$\overline{\omega}_{Olea,w}$ [b]	$\overline{\omega}_{Olea,AS,w}$ [b]	$g_{AS,w}$ [a]	$g_{Olea,w}$ [b]	$g_{Olea,AS,w}$ [b]	$RFE_{AS,w}/$ WAOD^{-1}m^{-2} [a]	$RFE_{Olea,w}/$ WAOD^{-1}m^{-2} [b]	$RFE_{Olea,AS,w}/$ WAOD^{-1}m^{-2} [b]
90	1.366+i0	1.545+i0.0012	1.449+i0.0012	0.97	0.97	0.81	0.75	0.73	-18.36	-20.00	-21.07
80	1.392+i0	1.570+i0.0012	1.493+i0.0012	0.97	0.97	0.81	0.76	0.67	-18.22	-19.81	-24.02
70	1.413+i0	1.581+i0.0012	1.520+i0.0012	0.98	0.97	0.74	0.77	0.71	-22.12	-19.43	-22.48
60	1.430+i0	1.589+i0.0012	1.538+i0.0012	0.98	0.97	0.71	0.78	0.74	-23.89	-18.69	-20.77
50	1.443+i0	1.602+i0.0012	1.557+i0.0012	0.98	0.97	0.72	0.78	0.75	-23.37	-18.80	-20.38
40	1.452+i0	1.621+i0.0012	1.577+i0.0012	0.98	0.97	0.65	0.77	0.73	-27.32	-19.14	-21.35

[a] Note: these values are given by Valenzuela et al. (2018).

[b] This study.

Table 2. $m, \overline{\omega}, g$ and RFE at 532 nm wavelength for AS, *Olea* and AS+*Olea* as function of RH calculated with conventional volume mixing rule for m of the mixture. We have omitted $\overline{\omega}$ for AS in table because it is equal to unit.

It is interesting to note that *Olea* pollen alone produces a lower cooling effect, practically independent of RH, compared to the radiative effects produced by AS alone. The difference is maximum for a relative humidity above 70% and extreme for a relative humidity of 90%, with a difference in *RFE* of around 8 WAOD^{-1}m^{-2} in absolute value. For the mixture of AS and *Olea* pollen, there is a maximum cooling effect at 80% RH, which is probably due to the lower value of the asymmetry parameter. Although *Olea* pollen contributes to the mixture with AS with a non-zero k, the weight of *n* becomes more important to the extent that it produces a greater cooling effect than *Olea* pollen alone. Therefore, the presence of *Olea* grains in the atmosphere may have an important thermoregulatory function.

If all pollen particles examined in this study cause a radiative effect like *Olea*, then there will be a population of bioaerosol particles that will decrease the cooling effect of pollen on radiative forcing efficiency. Better characterization of the n and k of ambient pollen is required to model its effects more accurately on climate, but even with k being non-zero it may affect climate differently than might be expected.

AUTHOR INFORMATION

Corresponding Author

[+,‡,*]**Antonio Valenzuela**- *Andalusian Institute for Earth System Research (IISTA-CEAMA) and Department of Applied Physics, University of Granada, Granada, 18071, Spain;* orcid.org/0000-0003-0290-4081; Email: avalenzuela@ugr.es

Author Contributions

The manuscript was written through contributions of all authors. All authors have given approval to the final version of the manuscript. [+,‡,ℵ]These authors contributed equally.

[+,‡]**Francisco José Garcia-Izquierdo**- *Andalusian Institute for Earth System Research (IISTA-CEAMA) and Department of Applied Physics, University of Granada, Granada, 18071, Spain;* orcid.org/0000-0002-0246-4648; Email: fragarizq@ugr.es

[+]**Gema Sánchez-Jiménez-** *Andalusian Institute for Earth System Research (IISTA-CEAMA);* Email: gemasj@ugr.es

[+,‡]**Elena Bazo**- *Andalusian Institute for Earth System Research (IISTA-CEAMA) and Department of Applied Physics, University of Granada, Granada, 18071, Spain;* orcid.org/0000-0003-1831-6874; Email: ebazo@ugr.es

[+,‡]**Juan Luis Guerrero-Rascado**- *Andalusian Institute for Earth System Research (IISTA-CEAMA) and Department of Applied Physics, University of Granada, Granada, 18071, Spain;* orcid.org/ 0000-0002-8317-2304; Email: rascado@ugr.es

[+,ℵ]**Paloma Cariñanos**- *Andalusian Institute for Earth System Research (IISTA-CEAMA) and* Department of Botany, University of Granada, Granada 18071, Spain orcid.org/ 0000-0002-8955-2383; Email: palomacg@ugr.es

[+,‡]**Lucas Alados-Arboledas**- *Andalusian Institute for Earth System Research (IISTA-CEAMA) and Department of Applied Physics, University of Granada, Granada, 18071, Spain;* orcid.org/ 0000-0003-3576-7167; Email: alados@ugr.es

[+,‡]**Francisco José Olmo-Reyes-** *Andalusian Institute for Earth System Research (IISTA-CEAMA) and Department of Applied Physics, University of Granada, Granada, 18071, Spain;* orcid.org/ 0000-0002-0186-1721; Email: fjolmo@ugr.es

Notes

The authors declare no competing financial interest.

ACKNOWLEDGMENTS

This work was supported by the Spanish Ministry of Science and Innovation through projects ELPIS (PID2020-12001-5RB-I00), by the Junta de Andalucía Excellence project ADAPNE (P20-00136), AEROPRE (P-18-RT-3820), FEDER Una manera de hacer Europa, EQC2019-006423-P, INTEGRATYON (PID2020-117825GB-C21 and PID2020-117825GB-C22), the European Union's Horizon 2020 research and innovation program through project ACTRIS.IMP (grant agreement No 871115), and ATMO-ACCESS (grant agreement No 101008004), , and ACTRIS-España (RED2022-134824-E), FEDER/Junta de Andalucía-Consejería de Transformación Económica, Industria, Conocimiento y Universidades project DEM3TRIOS (A-RNM-430-UGR20) and by University of Granada Plan Propio through Excellence Research Unit Earth Science and Singular Laboratory AGORA (LS2022-1) programs and project Pre-GREENMITIGATION (PP2022.PP.34).

Supporting Information

Additional information about cavity ring down time spectroscopy setup and the procedure to compare extinction cross section data from CRDS to data modelled with Mie theory; verification of our methodology by obtaining the optical properties of sodium chloride as a function of relative humidity.

REFERENCES

Bickel, W.S., Stafford, M.E., 1980. Biological particles as irregularly shaped scatterers, in: Light Scattering by Irregularly Shaped Particles. Springer, pp. 299–305.

Bielory, L., Lyons, K., Goldberg, R., 2012. Climate change and allergic disease. Curr Allergy Asthma Rep 12, 485–494. https://doi.org/10.1007/s11882-012-0314-z

Cholleton, D., Bialic, E., Dumas, A., Kaluzny, P., Rairoux, P., Miffre, A., 2022a. Laboratory evaluation of the scattering matrix of ragweed, ash, birch and pine pollen towards pollen classification. Atmos Meas Tech 15, 1021–1032. https://doi.org/10.5194/amt-15-1021-2022

Cholleton, D., Bialic, E., Dumas, A., Kaluzny, P., Rairoux, P., Miffre, A., 2022b. Laboratory evaluation of the scattering matrix of ragweed, ash, birch and pine pollen towards pollen classification. Atmos Meas Tech 15, 1021–1032. https://doi.org/10.5194/amt-15-1021-2022

Córdoba-Jabonero, C., Sicard, M., Ansmann, A., del Águila, A., Baars, H., 2018. Separation of the optical and mass features of particle components in different aerosol mixtures by using POLIPHON retrievals in synergy with continuous polarized Micro-Pulse Lidar (P-MPL) measurements. Atmos Meas Tech 11, 4775–4795. https://doi.org/10.5194/amt-11-4775-2018

Cotterell, M.I., Mason, B.J., Preston, T.C., Orr-Ewing, A.J., Reid, J.P., 2015. Optical extinction efficiency measurements on fine and accumulation mode aerosol using single particle cavity ring-down spectroscopy. Physical Chemistry Chemical Physics 17, 15843–15856. https://doi.org/10.1039/c5cp00252d

Cotterell, M.I., Willoughby, R.E., Bzdek, B.R., Orr-Ewing, A.J., Reid, J.P., 2017. A complete parameterisation of the relative humidity and wavelength dependence of the refractive index of hygroscopic inorganic aerosol particles. Atmos Chem Phys 17, 9837–9851. https://doi.org/10.5194/acp-17-9837-2017

David, G., Esat, K., Ritsch, I., Signorell, R., 2016. Ultraviolet broadband light scattering for optically-trapped submicron-sized aerosol particles. Physical Chemistry Chemical Physics 18, 5477–5485. https://doi.org/10.1039/c5cp06940h

Dawson, J.N., Malek, K.A., Razafindrambinina, P.N., Raymond, T.M., Dutcher, D.D., Asa-Awuku, A.A., Freedman, M.A., 2020. Direct Comparison of the Submicron Aerosol Hygroscopicity of Water-Soluble Sugars. ACS Earth Space Chem 4, 2215–2226. https://doi.org/10.1021/acsearthspacechem.0c00159

Deguillaume, L., Leriche, M., Amato, P., Ariya, P.A., Delort, A.-M., Pöschl, U., Chaumerliac, N., Bauer, H., Flossmann, A.I., Morris, C.E., 2008. Microbiology and atmospheric processes: chemical interactions of primary biological aerosols. Biogeosciences 5, 1073–1084. https://doi.org/10.5194/bg-5-1073-2008

Després, V.R., Alex Huffman, J., Burrows, S.M., Hoose, C., Safatov, A.S., Buryak, G., Fröhlich-Nowoisky, J., Elbert, W., Andreae, M.O., Pöschl, U., Jaenicke, R., 2012. Primary biological aerosol particles in the atmosphere: A review. Tellus B Chem Phys Meteorol 64. https://doi.org/10.3402/tellusb.v64i0.15598

Diehl, K., Quick, C., Matthias-Maser, S., Mitra, S.K., Jaenicke, R., 2001. The ice nucleating ability of pollen Part I: Laboratory studies in deposition and condensation freezing modes, Atmospheric Research.

Dinar, E., Riziq, A.A., Spindler, C., Erlick, C., Kiss, G., Rudich, Y., 2008. The complex refractive index of atmospheric and model humic-like substances (HULIS) retrieved by a cavity ring down aerosol spectrometer (CRD-AS). Faraday Discuss 137, 279–295.

Ebert, M., Weinbruch, S., Rausch, A., Gorzawski, G., Hoffmann, P., Wex, H., Helas, G., 2002. Complex refractive index of aerosols during LACE 98 as derived from the analysis of individual particles. Journal of Geophysical Research Atmospheres 107, 1–15. https://doi.org/10.1029/2000JD000195

Erlick, C., Abbatt, J.P.D., Rudich, Y., 2011. How different calculations of the refractive index affect estimates of the radiative forcing efficiency of ammonium sulfate aerosols. J Atmos Sci 68, 1845–1852.

Fernandez, M.O., Thomas, R.J., Garton, N.J., Hudson, A., Haddrell, A., Reid, J.P., 2019. Assessing the airborne survival of bacteria in populations of aerosol droplets with a novel technology. J R Soc Interface 16. https://doi.org/10.1098/rsif.2018.0779

Fröhlich-Nowoisky, J., Kampf, C.J., Weber, B., Huffman, J.A., Pöhlker, C., Andreae, M.O., Lang-Yona, N., Burrows, S.M., Gunthe, S.S., Elbert, W., Su, H., Hoor, P., Thines, E., Hoffmann, T., Després, V.R., Pöschl, U., 2016. Bioaerosols in the Earth system: Climate, health, and ecosystem interactions. Atmos Res. https://doi.org/10.1016/j.atmosres.2016.07.018

Garland, R.M., Ravishankara, A.R., Lovejoy, E.R., Tolbert, M.A., Baynard, T., 2007. Parameterization for the relative humidity dependence of light extinction : Organic-ammonium sulfate aerosol 112, 1–11. https://doi.org/10.1029/2006JD008179

Gómez Martín, J.C., Guirado, D., Frattin, E., Bermudez-Edo, M., Cariñanos Gonzalez, P., Olmo Reyes, F.J., Nousiainen, T., Gutiérrez, P.J., Moreno, F., Muñoz, O., 2021. On the application of scattering matrix measurements to detection and identification of major types of airborne aerosol particles: Volcanic ash, desert dust and pollen. J Quant Spectrosc Radiat Transf 271. https://doi.org/10.1016/j.jqsrt.2021.107761

Griffiths, P.T., Borlace, J.S., Gallimore, P.J., Kalberer, M., Herzog, M., Pope, F.D., 2012. Hygroscopic growth and cloud activation of pollen: A laboratory and modelling study. Atmospheric Science Letters 13, 289–295. https://doi.org/10.1002/asl.397

Haywood, J., Boucher, O., 2000. Estimates of the direct and indirect radiative forcing due to tropospheric aerosols: A review. Reviews of geophysics 38, 513–543.

Haywood, J.M., Shine, K.P., 1995. The effect of anthropogenic sulfate and soot aerosol on the clear sky planetary radiation budget. Geophys Res Lett 22, 603–606.

Hopkins, R.J., Mitchem, L., Ward, A.D., Reid, J.P., 2004. Control and characterisation of a single aerosol droplet in a single-beam gradient-force optical trap. Physical Chemistry Chemical Physics 6, 4924–4927. https://doi.org/10.1039/b414459g

Hu, Y., Zhao, X., Gu, Y., Chen, X., Wang, X., Wang, P., Zheng, Z., Dong, X., 2019. Significant broadband extinction abilities of bioaerosols. Sci China Mater. https://doi.org/10.1007/s40843-018-9411-9

Huffman, J.A., Santarpia, J., 2017. Online techniques for quantification and characterization of biological aerosols. Microbiology of aerosols 83–114.

Hulst, Hendrik Christoffel, van de Hulst, Hendrik C, 1981. Light scattering by small particles. Courier Corporation.

Kim, G., Lee, S.Y., Shin, S., Park, Y.K., 2018. Three-dimensional label-free imaging and analysis of Pinus pollen grains using optical diffraction tomography. Sci Rep 8, 1–8. https://doi.org/10.1038/s41598-018-20113-w

Kiselev, D., Bonacina, L., Wolf, J.P., 2013. A flash-lamp based device for fluorescence detection and identification of individual pollen grains. Review of Scientific Instruments 84. https://doi.org/10.1063/1.4793792

Knight, J.W., Egan, J. V., Orr-Ewing, A.J., Cotterell, M.I., 2022. Direct Spectroscopic Quantification of the Absorption and Scattering Properties for Single Aerosol Particles. Journal of Physical Chemistry A 126, 1571–1577. https://doi.org/10.1021/acs.jpca.2c00532

Krieger, U.K., Marcolli, C., Reid, J.P., 2012. Exploring the complexity of aerosol particle properties and processes using single particle techniques. Chem Soc Rev 41, 6631–6662. https://doi.org/10.1039/c2cs35082c

L. Price, C., Bain, A., J. Wallace, B., C. Preston, T., F. Davies, J., 2020. Simultaneous Retrieval of the Size and Refractive Index of Suspended Droplets in a Linear Quadrupole Electrodynamic Balance. J Phys Chem A 124, 1811–1820. https://doi.org/10.1021/acs.jpca.9b10748

Martin, S.T., Andreae, M.O., Artaxo, P., Baumgardner, D., Chen, Q., Goldstein, A.H., Guenther, A., Heald, C.L., Mayol-Bracero, O.L., McMurry, P.H., Pauliquevis, T., Pschl, U., Prather, K.A., Roberts, G.C., Saleska, S.R., Silva Dias, M.A., Spracklen, D. V., Swietlicki, E., Trebs, I., 2010. Sources and properties of Amazonian aerosol particles. Reviews of Geophysics 48. https://doi.org/10.1029/2008RG000280

Mason, B.J., Cotterell, M.I., Preston, T.C., Orr-Ewing, A.J., Reid, J.P., 2015. Direct measurements of the optical cross sections and refractive indices of individual volatile and hygroscopic aerosol particles. J Phys Chem A 119, 5701–5713.

Matthias-Maser, S., Bogs, B., Jaenicke, R., 2000. The size distribution of primary biological aerosol particles in cloud water on the mountain Kleiner Feldberg/Taunus (FRG). Atmos Res 54, 1–13. https://doi.org/10.1016/S0169-8095(00)00039-9

McCartney, E.J., 1976. Optics of the atmosphere: scattering by molecules and particles. nyjw.

Möhler, O., DeMott, P.J., Vali, G., Levin, Z., 2007. Microbiology and atmospheric processes: the role of biological particles in cloud physics. Biogeosciences 4, 1059–1071. https://doi.org/10.5194/bg-4-1059-2007

Moller, B., Rarey, J., Ramjugernath, D., 2008. Estimation of the vapour pressure of non-electrolyte organic compounds via group contributions and group interactions. J Mol Liq 143, 52–63. https://doi.org/10.1016/j.molliq.2008.04.020

Noh, Y.M., Lee, H., Mueller, D., Lee, K., Shin, D., Shin, S., Choi, T.J., Choi, Y.J., Kim, K.R., 2013a. Investigation of the diurnal pattern of the vertical distribution of pollen in the lower troposphere using LIDAR. Atmos Chem Phys 13, 7619–7629. https://doi.org/10.5194/acp-13-7619-2013

Noh, Y.M., Lee, H., Mueller, D., Lee, K., Shin, D., Shin, S., Choi, T.J., Choi, Y.J., Kim, K.R., 2013b. Investigation of the diurnal pattern of the vertical distribution of pollen in the lower troposphere using LIDAR. Atmos Chem Phys 13, 7619–7629. https://doi.org/10.5194/acp-13-7619-2013

Noll&Khalili, E. (1988). *Atmospheric Environment* (Vol. 22, Issue 3).

O'Connor, D.J., Iacopino, D., Healy, D.A., O'Sullivan, D., Sodeau, J.R., 2011. The intrinsic fluorescence spectra of selected pollen and fungal spores. Atmos Environ 45, 6451–6458. https://doi.org/10.1016/j.atmosenv.2011.07.044

Pan, Y. Le, Hill, S.C., Pinnick, R.G., House, J.M., Flagan, R.C., Chang, R.K., 2011. Dual-excitation-wavelength fluorescence spectra and elastic scattering for differentiation of single airborne pollen and fungal particles. Atmos Environ 45, 1555–1563. https://doi.org/10.1016/j.atmosenv.2010.12.042

Petters, M.D., Kreidenweis, S.M., 2007. A single parameter representation of hygroscopic growth and cloud condensation nucleus activity.

Pope, F.D., 2010a. Pollen grains are efficient cloud condensation nuclei. Environmental Research Letters 5. https://doi.org/10.1088/1748-9326/5/4/044015

Pope, F.D., 2010b. Pollen grains are efficient cloud condensation nuclei. Environmental Research Letters 5. https://doi.org/10.1088/1748-9326/5/4/044015

Prisle, N. L., Lin, J. J., Purdue, S., Lin, H., Carson Meredith, J., & Nenes, A. (2019). Cloud condensation nuclei activity of six pollenkitts and the influence of their surface activity. *Atmospheric Chemistry and Physics*, *19*(7), 4741–4761. https://doi.org/10.5194/acp-19-4741-2019

Ramírez-Aliaga, P., Foyo-Moreno, I., Cariñanos, P., 2022. Effects of Environmental Stress on the Pollen Viability of Ornamental Tree-Species in the City of Granada (South-Eastern Spain). Forests 13. https://doi.org/10.3390/f13122131

Randles, C.A., Russell, L.M., Ramaswamy, V., 2004. Hygroscopic and optical properties of organic sea salt aerosol and consequences for climate forcing. Geophys Res Lett 31.

Redding, B., Pan, Y.-L., 2015a. Optical trap for both transparent and absorbing particles in air using a single shaped laser beam. Opt Lett 40, 2798–2801.

Redding, B., Pan, Y.-L., 2015b. Optical trap for both transparent and absorbing particles in air using a single shaped laser beam. Opt Lett 40, 2798. https://doi.org/10.1364/ol.40.002798

Robinson, C. B., Schill, G. P., Zarzana, K. J., & Tolbert, M. A. (2013). Impact of organic coating on optical growth of ammonium sulfate particles. *Environmental Science and Technology*, *47*(23), 13339–13346. https://doi.org/10.1021/es4023128

Santarpia, J.L., 2016. Bioaerosols in the environment: Populations, measurement, and processes, In Aerobiology: The Toxicology of Airborne Pathogens and Toxins, in: Aerobiology: The Toxicology of Airborne Pathogens and Toxins.

Sassen, K., 2008. Boreal tree pollen sensed by polarization lidar: Depolarizing biogenic chaff. Geophys Res Lett 35, L18810. https://doi.org/10.1029/2008GL035085

Shang, X., Giannakaki, E., Bohlmann, S., Filioglou, M., Saarto, A., Ruuskanen, A., Leskinen, A., Romakkaniemi, S., Komppula, M., 2020. Optical characterization of pure pollen types using a multi-wavelength Raman polarization lidar. Atmos Chem Phys 20, 15323–15339. https://doi.org/10.5194/acp-20-15323-2020

Sicard, M., Izquierdo, R., Alarcón, M., Belmonte, J., Comerón, A., Baldasano, J.M., 2016. Near-surface and columnar measurements with a micro pulse lidar of atmospheric pollen in Barcelona, Spain. Atmos Chem Phys 16, 6805–6821. https://doi.org/10.5194/acp-16-6805-2016

Stocker, T.F., Qin, D., Plattner, G.-K., Tignor, M., Allen, S.K., Boschung, J., Nauels, A., Xia, Y., Bex, V., Midgley, P.M., 2013. Climate change 2013: The physical science basis. Contribution of working group I to the fifth assessment report of the intergovernmental panel on climate change 1535.

Swanson, B., Freeman, M., Rezgui, S., Huffman, J.A., 2023. Pollen classification using a single particle fluorescence spectroscopy technique. Aerosol Science and Technology 57, 112–133. https://doi.org/10.1080/02786826.2022.2142510

Tang, M., Gu, W., Ma, Q., Jie Li, Y., Zhong, C., Li, S., Yin, X., Huang, R.J., He, H., Wang, X., 2019. Water adsorption and hygroscopic growth of six anemophilous pollen species: The effect of temperature. Atmos Chem Phys 19, 2247–2258. https://doi.org/10.5194/acp-19-2247-2019

Valenzuela, A., Bazo, E., Rica, R.A., Alados-Arboledas, L., Olmo-Reyes, F.J., 2024. Electrodynamic single-particle trap integrated into double-cavity ring-down spectroscopy for light extinction. J Aerosol Sci 175, 106292. https://doi.org/10.1016/j.jaerosci.2023.106292

Valenzuela, A., Chu, F., Haddrell, A., Cotterell, M., Walker, J., Orr-Ewing, A., Reid, J., 2021. Optical Interrogation of Single Levitated Droplets in a Linear Quadrupole Trap by Cavity Ring-Down Spectroscopy. J Phys Chem A 125, 394–405. https://doi.org/10.1021/acs.jpca.0c09213

Valenzuela, A., Reid, J.P., Bzdek, B.R., Orr-Ewing, A.J., 2018. Accuracy Required in Measurements of Refractive Index and Hygroscopic Response to Reduce Uncertainties in Estimates of Aerosol Radiative Forcing Efficiency. Journal of Geophysical Research: Atmospheres 123, 6469–6486. https://doi.org/10.1029/2018JD028365

Valenzuela, A., Rica, R.A., Olmo-Reyes, F.J., Alados-Arboledas, L., 2020. Testing a Paul trap through determining the evaporation rate of levitated single semi-volatile organic droplets. Opt Express 28, 34812. https://doi.org/10.1364/OE.410590

Walker, J.S., Carruthers, A.E., Orr-Ewing, A.J., Reid, J.P., 2013. Measurements of light extinction by single aerosol particles. J Phys Chem Lett 4, 1748–1752.

Wang, C., Pan, Y. Le, Hill, S.C., Redding, B., 2015. Photophoretic trapping-Raman spectroscopy for single pollens and fungal spores trapped in air. J Quant Spectrosc Radiat Transf 153, 4–12. https://doi.org/10.1016/j.jqsrt.2014.11.004

Wang, Z., Bi, L., Yi, B., Zhang, X., 2019. How the Inhomogeneity of Wet Sea Salt Aerosols Affects Direct Radiative Forcing. Geophys Res Lett 46, 1805–1813. https://doi.org/10.1029/2018GL081193

Wiscombe, W.J., Grams, G.W., 1976. The backscattered fraction in two-stream approximations. J Atmos Sci 33, 2440–2451.

Zarzana, K.J., Cappa, C.D., Tolbert, M.A., 2014. Sensitivity of aerosol refractive index retrievals using optical spectroscopy. Aerosol Science and Technology 48, 1133–1144.

Zarzana, K.J., De Haan, D.O., Freedman, M.A., Hasenkopf, C.A., Tolbert, M.A., 2012. Optical properties of the products of α-dicarbonyl and amine reactions in simulated cloud droplets. Environ Sci Technol 46, 4845–4851. https://doi.org/10.1021/es2040152

Zhang, M., Khaled, A., Amato, P., Delort, A.-M., Ervens, B., 2021. Sensitivities to biological aerosol particle properties and ageing processes: potential implications for aerosol–cloud interactions and optical properties. Atmos Chem Phys 21, 3699–3724. https://doi.org/10.5194/acp-21-3699-2021

Ziska, L., Knowlton, K., Rogers, C., Dalan, D., Tierney, N., Elder, M.A., Filley, W., Shropshire, J., Ford, L.B., Hedberg, C., Fleetwood, P., Hovanky, K.T., Kavanaugh, T., Fulford, G., Vrtis, R.F., Patz, J.A., Portnoy, J., Coates, F., Bielory, L., Frenz, D., 2011. Recent warming by latitude associated with increased length of ragweed pollen season in central North America. Proc Natl Acad Sci U S A 108, 4248–4251. https://doi.org/10.1073/pnas.1014107108

Cavity ring down time measurements were measured for single pollen particles for the first time.

The dependency on relative humidity was calculated for extinction cross sections.

Refractive index was retrieved from the fit with Mie theory

The authors declare that they have no known competing financial interests or personal relationships that could have appeared to influence the work reported in this paper.